

Supporting Information for

Understanding the Swelling Behavior of Modified Nano-Clay Filler Particles in Water and Ethanol

Sebastian Metz^{*a}, *Richard L. Anderson*^a, *Dawn L. Geatches*^a, *James L. Suter*^b, *Robert Lines*^c, and *H. Chris Greenwell*^{*d}

^a Hartree Centre, STFC Daresbury Laboratory, Scientific Computing Department, Sci-Tech Daresbury, Keckwick Lane, Daresbury, Warrington WA4 4AD

^b Centre for Computational Science, Department of Chemistry, University College London, 20 Gordon Street, London, UK

^c Sun Chemical Ltd, St. Mary Cray Technical Centre, Cray Avenue, St. Mary Cray, Orpington, Kent, BR5 3PP, UK

^d Department of Earth Sciences, Durham University, Science Labs, South Road, Durham, DH1 3LE, UK

*corresponding authors: sebastian.metz@stfc.ac.uk
chris.greenwell@durham.ac.uk

Computational details

We used the LAMMPS version from 20th October 2012; in all calculations, we used style=real, the corresponding system parameters are given below in Tables S1-S4

Table S1: Molecule group, atom types (based on the CVFF force field nomenclature used for the bonding parameters, see Tables S2-S4), partial charges and pair coefficients (based on CHARMM parameters) for all atoms present in ethanol and the molecules Q_{A-C}. The non-bonded interactions are calculated by

$$E = 4\epsilon \left[\left(\frac{\sigma}{r} \right)^{12} - \left(\frac{\sigma}{r} \right)^6 \right]$$

Group	Type	Charge	ϵ /(kcal/mol)	σ /Å
<u>C</u> H ₃	C3	-0.27	0.0380000	2.4500
<u>C</u> H ₃	Hc	0.09	0.0390000	3.8754
<u>C</u> H ₂	C2	-0.18	0.0380000	2.4500
<u>C</u> H ₂	Hc	0.09	0.0390000	3.8754
[N(<u>C</u> H ₂) ₃ (<u>C</u> H ₃)] ⁺	N4	-0.60	0.1670000	3.5012
[N(<u>C</u> H ₂) ₃ (<u>C</u> H ₃)] ⁺	Cn	-0.10	0.0390000	3.8754
[N(<u>C</u> H ₂) ₃ (<u>C</u> H ₃)] ⁺	H	0.25	0.0380000	2.4500
[N(<u>C</u> H ₂) ₃ (<u>C</u> H ₃)] ⁺	Cn	-0.35	0.0390000	3.8754
[N(<u>C</u> H ₂) ₃ (<u>C</u> H ₃)] ⁺	H	0.25	0.0380000	2.4500
<u>C</u> H ₂ -O- <u>C</u> H ₂	C2	-0.01	0.0390000	3.8754
<u>C</u> H ₂ -O- <u>C</u> H ₂	Hc	0.09	0.0380000	2.4500
<u>C</u> H ₂ -O- <u>C</u> H ₂	Oc	-0.34	0.2280000	2.8598
<u>C</u> H ₂ -OH	C2	0.05	0.0390000	3.8754
<u>C</u> H ₂ -OH	Hc	0.09	0.0380000	2.4500
<u>C</u> H ₂ -OH	Oh	-0.66	0.1554000	3.1655
<u>C</u> H ₂ -O <u>H</u>	ho	0.43	0.0	0.0

Table S2: Parameter for all bonds present in ethanol and in the molecules Q_{A-C} using the harmonic bond energy expression: $E = k_{bond}(r - r_0)^2$

Bond type	k_{bond} /(kcal/(mol *Å ²))	r_0 /Å
C3-C2	322.7158	1.526
C2-C2	322.7158	1.526
C3-Hc	340.6175	1.105
C2-Hc	340.6175	1.105
Cn-H	340.6175	1.105
Cn-N4	356.5988	1.470
C2-Oc	273.2000	1.425
C2-Oh	384.0000	1.420
Oh-Ho	540.6336	0.960

Table S3: Parameter for all angles present in ethanol and the molecules Q_{A-C} using the harmonic angle energy expression: $E = k_{angle}(\theta - \theta_0)^2$

Angle-type	$k_{angle}/(\text{kcal}/(\text{mol} * \text{degree}^2))$	θ_0/degree
C3-C2-C2	46.6000	110.5000
C2-C2-C2	46.6000	110.5000
C3-C2-Hc	44.4000	110.0000
C2-C3-Hc	44.4000	110.0000
C2-C2-Hc	44.4000	110.0000
C2-C2-H	44.4000	110.0000
C2-Cn-N4	50.0000	109.5000
C2-C2-Oc	70.0000	109.5000
C2-C2-Oh	70.0000	109.5000
Cn-N4-Cn	86.3000	112.0000
C2-Oc-C2	70.0000	109.5000
C2-Oh-Ho	70.0000	109.5000
Hc-C2-Oc	57.0000	109.5000
Hc-C2-Oh	57.0000	109.5000
Hc-C2-N4	57.0000	109.5000
Hc-C3-Hc	39.5000	106.4000
Hc-C2-Hc	39.5000	106.4000
H-C2-H	39.5000	106.4000

Table S4: Parameter for all dihedrals present in ethanol and the molecules Q_{A-C} using the harmonic dihedral energy expression: $E = k_{dihedral}[1 + d * \cos(n\phi)]$

Dihedral-type	$k_{dihedral}/(\text{kcal}/\text{mol})$	d	n
C2-C2-C2-C3	0.1581	1	3
C2-C2-C2-C2	0.1581	1	3
C2-C2-C2-Cn	0.1581	1	3
C2-C2-C3-Hc	0.1581	1	3
C2-C2-C2-Hc	0.1581	1	3
Cn-C2-C2-Hc	0.1581	1	3
C2-C2-Cn-H	0.1581	1	3
C3-C2-C2-Hc	0.1581	1	3
Hc-C2-C2-Hc	0.1581	1	3
Hc-C2-C3-Hc	0.1581	1	3
Hc-C2-Cn-H	0.1581	1	3
Oc-C2-C2-Hc	0.1581	1	3
Oc-C2-Cn-H	0.1581	1	3
Oh-C2-C2-Hc	0.1581	1	3
Oh-C2-Cn-H	0.1581	1	3
Oc-C2-C2-Oc	0.1581	1	3
Oc-C2-C2-Oh	0.1581	1	3
Oc-C2-Cn-N4	0.1581	1	3
Oh-C2-Cn-N4	0.1581	1	3
C2-C2-Oc-C2	0.1300	1	3
Cn-C2-Oc-C2	0.1300	1	3
C2-C2-Oh-Ho	0.1300	1	3
Cn-C2-Oh-Ho	0.1300	1	3
C2-Oc-C2-Hc	0.1300	1	3
Hc-C2-Oh-Ho	0.1300	1	3
Cn-N4-Cn-C2	0.0889	1	3
Cn-N4-Cn-H	0.0889	1	3

We cross checked the validity of the above parameters by comparing the density of a box of ethanol molecules for different temperatures. The results [$\rho(273\text{K})=0.8345\text{g/cm}^3$, $\rho(293\text{K})=0.8225\text{g/cm}^3$ and $\rho(298\text{K})=0.8184\text{g/cm}^3$] reproduce the experimentally observed trend of lower density with higher temperatures quite accurately and overestimate the experimentally determined values¹ at the different temperatures [$\rho(273\text{K})=0.8062\text{g/cm}^3$, $\rho(293\text{K})=0.7892\text{g/cm}^3$ and $\rho(298\text{K})=0.7850\text{g/cm}^3$] by about 4% and the values of the OPLS forcefield² at room temperature [$\rho(298\text{K})=0.799\text{g/cm}^3$] by only 2.5%. While it would be very simple to slightly modify the nonbonding parameters to accurately match the density, the nonbonding parameters were kept consistent with the quaternary ions, which have to be considered to be of higher importance.

Automation details

1. Initial models were created through random insertion of organic molecules and water (or ethanol) corresponding to a solvation state of 500 mg solvent per g clay in the interlayer space at a very low density (atom number density 0.05 \AA^{-3}). This starting system was created by expanding the clay sheet separation to give the volume required for the specified atom number density, followed by insertion of organic molecules with random position and orientation (ensuring no overlap with clay framework atoms or previously inserted organic molecules). The interlayer spacing was then mapped onto a grid of approximately 2.5 \AA spacing; solvent molecules were inserted at grid points which were not covered by the organic molecules (or ethanol molecules) with random orientation until the required amount of water (or ethanol) was added. These low-density initial systems were far from equilibrium. Therefore the clay systems were treated with a simulated annealing approach; each system was heated to 400 K in a molecular dynamics simulation over 10 ps, simulated at 400 K for 50 ps, then cooled down to 300 K over 10 ps. The system was then simulated using molecular dynamics at 300 K initially for 1.5 ns with the final 0.5 ns used for data collection. Equilibrium was determined to have occurred when there is no drift in the potential energy and d -spacings.

2. Further solvation states were investigated sequentially for each of these inhibitor molecules by randomly deleting water molecules at the end of each molecular dynamics simulation to create a lower hydration state, in steps of 25 mg of solvent per g clay.

3. The ensuing solvation states, derived from a higher solvation state, were simulated for 1 ns at 300 K, again with the last 0.5 ns used for data collection.

4. This procedure was continued until all solvent was removed and the dry clay–polymer system was finally simulated. This results in a minimum of 21 linked simulations for each clay system. As each new simulation was set up from an equilibrated, preceding one, each clay system was simulated over the course of the solvation simulations for upwards of 30 ns.

5. Further solvation states were also explored where it was deemed suitable.

1-D plots: The location of the atoms of solvent, Na⁺ cations and surfactants were determined using 1-dimensional atom density plots for different solvent loadings, created by dividing the simulation cell into slices 0.01nm along the *z*-direction i.e. perpendicular to the clay sheets. The density of each atom type present in each of these slices was then averaged across the last 0.5ns of simulation time.

d-spacing: By considering the points of inflection in the *d*-spacing curves and changes in the 1-D density profile perpendicular to the clay sheets, we will see in the following sections, that for the three investigated Na⁺-clays, the solvent coverages correspond to a mono-layer, (0-125mg solvent/g clay) a bi-layer, (125-250 mg solvent/g clay) a tri-layer, (250-375 mg solvent/g clay) and a quadri-layer (375-500 mg solvent/g clay).

Solvation energetics: Conceptually, the interlayer spacing of clay mineral is a subtle balance of the repulsive forces felt by two similarly charged clay platelets versus the attraction of these layers for oppositely charged interlayer cations, moderated by any solvent that may screen those charges.

Assuming that entropic forces have a negligible contribution to free energy of swelling,³ then the process is dominated by the energetics. Kalinichev and colleagues defined a hydration energy as the difference between the energy of the solvated interlayer and the same interlayer with no solvent present, normalized to the number of solvent molecules:

$$\Delta U_H(N) = \frac{\langle U(N) - U(0) \rangle}{N}$$

where $\langle U(N) \rangle$ and $\langle U(0) \rangle$ are the average potential energies of an equilibrated, solvated system and equilibrated,⁴ dry system (as a reference solvation state) respectively.

However, this original definition, though effective for highly charged layered double hydroxides with high charge density anions (chloride), when tested by Suter *et al.* appeared to predict infinite swelling in most clay systems.³ This is due to the fact that the initial solvation of totally solvent free clay interlayers was so energetically favourable that the energy contribution from this by far exceeded subsequent solvation. As such, a model was proposed accounting for a layer-by-layer solvation energy:

$$\Delta U(\text{monolayer})(N) = \frac{\langle U(N) - U(0) \rangle}{N}$$

$$\Delta U(\text{bilayer})(N) = \frac{\langle U(N) - U(\text{full monolayer}) \rangle}{N - N(\text{full monolayer})}$$

$$\Delta U(\text{trilayer})(N) = \frac{\langle U(N) - U(\text{full bilayer}) \rangle}{N - N(\text{full bilayer})}$$

If a solvent free clay system is considered, the individual layers will be only separated by the interlayer cations, and vacuum. Initially, solvent molecules will fill up the space available, solvating cations and the clay surfaces until all space is filled and a monolayer of solvent exists. During this process the interlayer spacing remains unchanged. In order to fit any more solvent in, for example to fully solvate the cations, the interlayer must now expand; however this requires the whole interlayer to expand thereby increasing the amount of free space dramatically and resulting in an abrupt increase in interlayer space. This space then continues to fill with solvent, with little change in d -spacing until it is saturated. This stepwise transition continues for a bilayer of solvent and even a tri-layer, though beyond this the steps in d -spacing become less distinct owing to there being much more configuration space available to accommodate further solvent. By measuring the potential energy of step-wise solvated systems, and scaling this by the number of solvent molecules, we were able to obtain solvation energetics, which were then compared to the potential energy of bulk solvent to determine the point at

which further swelling was energetically unfavorable. The (001) interlayer spacing, i.e. basal d -spacing of the silicate layers of the clay minerals was calculated every 0.5ps. Further details of the theory behind the calculation of solvation energies can be found in reference 4.

Solvent structure at high loading

To elucidate the interlayer structure of the surfactant/solvent mix in more detail the following presents results at a solvent loading of 450 mg/g clay. At this point the d -spacing and solvation energetics confirm that these trends are already well-established and sufficiently described above, so the following focusses on the 1-D atom density plots shown in Figures S1 and S2.

Montmorillonite and Surfactant Q_{A-C} solvated at 450 mg/g clay in water and ethanol

In all three cases, the water is structured most adjacent to the clay surface. While there remains some degree of ordering in the mid-plane of the interlayer in the case of Q_A , this ordering is much less pronounced for Q_B and nearly non-existing in Q_C , coinciding with the number of short C_2H_4-OH groups (0 in Q_A , 1 in Q_B and 2 in Q_C) in the different quaternary ammonium ions.

For all three water systems, a small amount of the ammonium groups can be found towards the middle of the interlayer, hydrated by water, but they mostly reside closer to the clay layers. The CH_3 terminated alkylic side-chains of the Q cations in MMT tend, on average, to prefer to be close to the clay layers. This is not surprising owing to the hydrophilic nature of the interlayer in the water systems. To a certain extent, however, they reach out into the interlayer region, forming areas with a slightly increased probability of finding the CH_3 groups, partially reflecting the structure of the solvent.

In ethanol, MMT- Q_{A-C} all differ in the ordering of the surfactant groups. The end group of the hydrophobic alkyl chains in all three cases has a still existing, but strongly reduced tendency to be located at the clay interface. In the case of Q_A and Q_B a more indistinct area toward the mid-plane of the interlayer is formed, while in the case of Q_C , the end group of the hydrophobic alkyl chain forms a distinct quadri-layer within the interlayer mid-plane, coinciding with the CH_2 and CH_3 groups of

ethanol. The ammonium groups for Q_{A-C} sit close to the clay layers, strongly attracted by the net negatively charged clay surface. Unlike the water solvent systems, no ammonium groups enter the middle section of the interlayer in the ethanol systems. For Q_C , with no ether groups, but only two C_2H_4OH groups, the O atoms form three distinct peaks close to the clay surface, intruding inside (closer to the clay than) the N atoms density peak. Q_A has two side-chains with 4 ether-groups and forms two distinct layers close to each surface tailing off towards the interlayer mid-plane. Q_B has the longer ether side-chain (eight ether groups) and its O atoms form five semi-distinct layers across the interlayer. This is at a cost though, with less density of O atoms at the clay surface. The effect of these observations on the energetics of separating the clay layers remains to be elucidated and is beyond the scope of this study.

It is noteworthy in this context, that even at these high solvent loadings, ethanol still shows a high degree of ordering in 7 layers (for Q_A and Q_B) or 6 layers (Q_C). This is most likely to remain true for even higher solvent loadings, as demonstrated in the case of MMT- Q_A with 750 mg ethanol per gram clay, where nine layers of ethanol are formed (see below).

The density profiles highlight that the most significant difference in the interlayer behavior occurs according to the length of the ether side-chains. With its longer side-chain, Q_B is able to influence the structure of the middle of the interlayer region far more than that of Q_A , which does so more than Q_C . These differences do not, however, alter significantly the behavior of ethanol in the interlayer region. The layers formed by ethanol in the interlayer are more distinct than those formed by water at the same solvent loading.

Vermiculite and Surfactant Q_{A-C} solvated at 450 mg/g clay in water and ethanol

In contrast to the MMT systems, there are fewer differences within the structures of the solvent in these systems. In both the VMT- Q_A and VMT- Q_B case, the water is structured most adjacent to the clay surface, with a broader, but high density in the mid-plane of the interlayer. Q_A , which has lower density

of ether O atoms in the mid-plane (due to two shorter ether side-chains compared to one long and a short one in Q_B), has a higher water concentration at the mid-plane. In the Q_C-VMT water system the water is more ordered close to the clay surfaces and around the hydroxyl groups of Q_C (which – due to the length of the chains - are close to the surface, too). Apart from this ordering close to the surface, the water molecules occupy the rest of the interlayer region fairly homogeneously.

For the water systems, the structures of the hydrated surfactants show similar behavior forming more (for Q_A with two ether side-chains of four ether units) or less (for Q_B with only one ether side chain consisting of eight ether units) structured layers of ether oxygens. The CH₃ end groups of the hydrophobic alkyl chain are located at either side of the mid-plane of the interlayer, proving that the hydrophobic alkyl chain points away from the clay surface too. In contrast to this, the CH₃ end groups of the hydrophobic alkyl chain in Q_C are much more uniformly spread in the interlayer region. The O of the hydroxyl group of Q_C lies closer to the clay surfaces than the N group, and extends to two well-defined layers away from the surface before rapidly tailing off towards the center of the interlayer region for Q_A and Q_B. For both, the ether side-chains point perpendicularly away from the clay surface,

For the VMT-Q systems in ethanol, Q_A and Q_B show essentially the same similarities and differences as for the water systems: For both, the CH₃ end groups of the hydrophobic alkyl chain at the interface of the surfactant with the solvent filled mid-plane region of the interlayer, proving that the hydrophobic alkyl chain points away from the clay surface. The ether side-chains also point perpendicularly away from the clay surface, forming more (for Q_A with two ether side-chains of four ether units) or less (for Q_B with only one ether side chain consisting of eight ether units) structured layers of ether oxygen. In the Q_A system, there is very little density of the ether oxygen in the region around the mid-plane interlayer, mainly owing to the ether side-chains being restricted in length. The O of the hydroxyl groups of Q_C lie close to the clay surfaces, forming an asymmetric double peak and suggesting that there are two different alignments of the C₂H₄OH groups. As the oxygen peaks sandwich the N ammonium group, this is assigned to charge stabilization effects. The CH₃ head group of the

hydrophobic side-chain in Q_C (which is longer than the hydrophobic side chains in Q_A and Q_B) lies more towards the center of the interlayer, with the whole surfactant being completely solvated by ethanol.

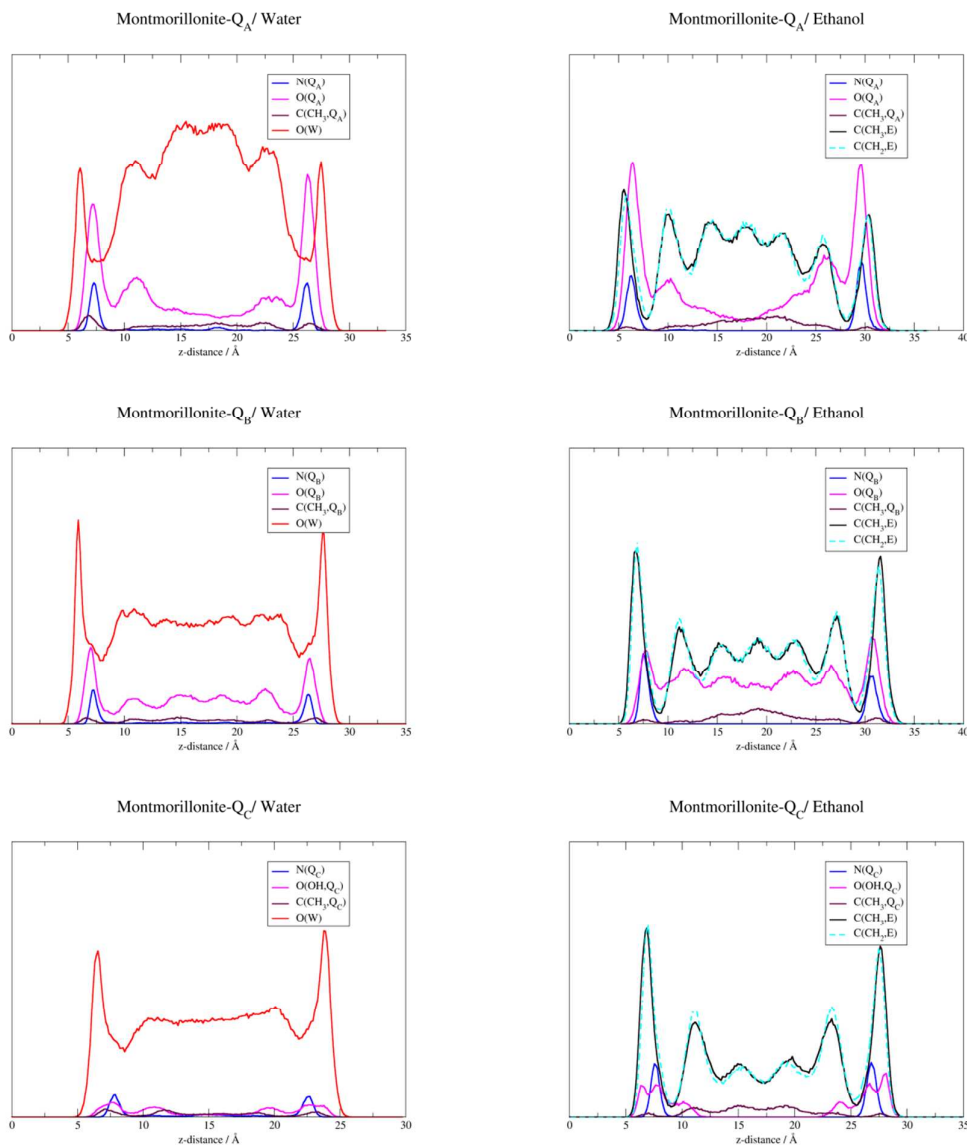


Figure S1. 1D-plots for the three MMT- Q_A -C systems at 450 mg/g clay solvent loading using water (left) or ethanol (right) as solvent. $C(CH_3, Q_{A/B/C})$ denotes the end group of the hydrophobic tail, $O(Q_{A/B})$ the oxygen atoms of the ether groups, $OH(Q_C)$ the oxygen atoms of the alcoholic end groups, $O(W)$ the oxygen atom of the water molecules and $C(CH_3, E)$ and $C(CH_2, E)$ the two different carbon atoms in ethanol.

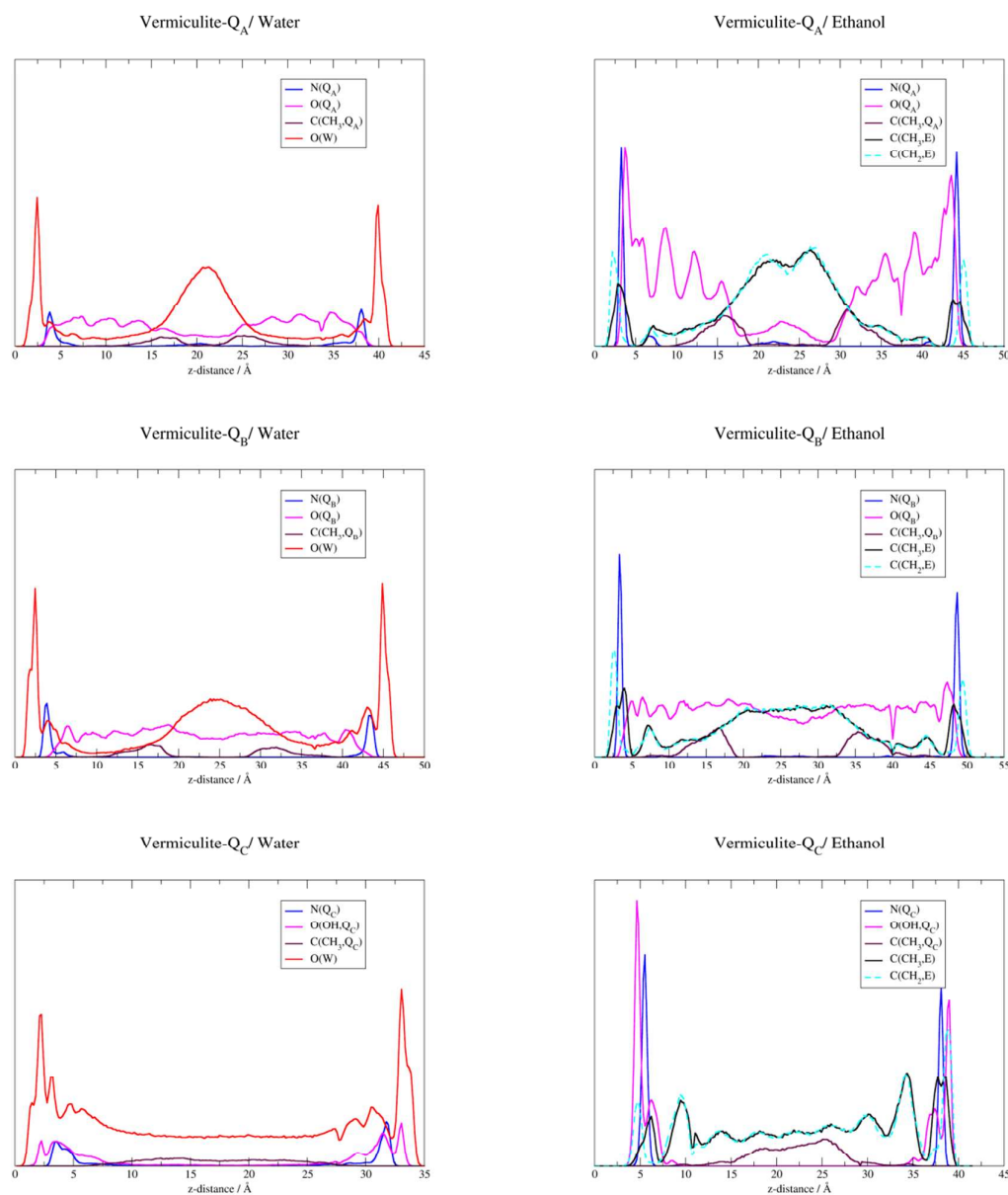


Figure S2. 1D-plots for the three VMT- Q_{A-C} systems at 450 mg/g clay solvent loading using water (left) or ethanol (right) as solvent. $C(\text{CH}_3, Q_{A/B/C})$ denotes the end group of the hydrophobic tail, $O(Q_{A/B})$ the oxygen atoms of the ether groups, $\text{OH}(Q_C)$ the oxygen atoms of the alcoholic end groups, $O(W)$ the oxygen atom of the water molecules and $C(\text{CH}_3, E)$ and $C(\text{CH}_2, E)$ the two different carbon atoms in ethanol.

The density profiles highlight that Q_A and Q_B share many similarities, with a significant difference in the interlayer behavior according to the length of the ether side-chains. With its shorter side-chain, Q_A seems to impose a stronger ordering of the solvent molecules in the middle of the interlayer region,

expressed in a sharper central peak for water as solvent and a structured double peak for ethanol as solvent. The effects of Q_C are much more dependent on the solvent: while there is almost no ordering in the water structure apart from the direct surface peak, ethanol forms – apart from the surface peaks – seven distinctive layers in the interlayer region.

To establish how far from equilibrium the interlayer and external bulk solvent were in the MMT-Q systems, the one that appeared closest to the bulk solvent energy, MMT- Q_A , was run at a higher solvent weight of 750 mg of solvent per g of clay. The extended clay swelling energetics for the MMT- Q_A system in ethanol is shown in Figure S3 and the 1D plots for the 750 mg ethanol per g of MMT is displayed in Figure S4. It can be seen that though the system appeared to be equilibrating at 500 mg of solvent per g of clay, the system only just surpasses the bulk solvent energy at 750 mg of solvent per g of clay. From S4 it can be seen that even at this high load of solvent, residual structuring of the ethanol is clearly evident, suggesting full exfoliation has not yet occurred.

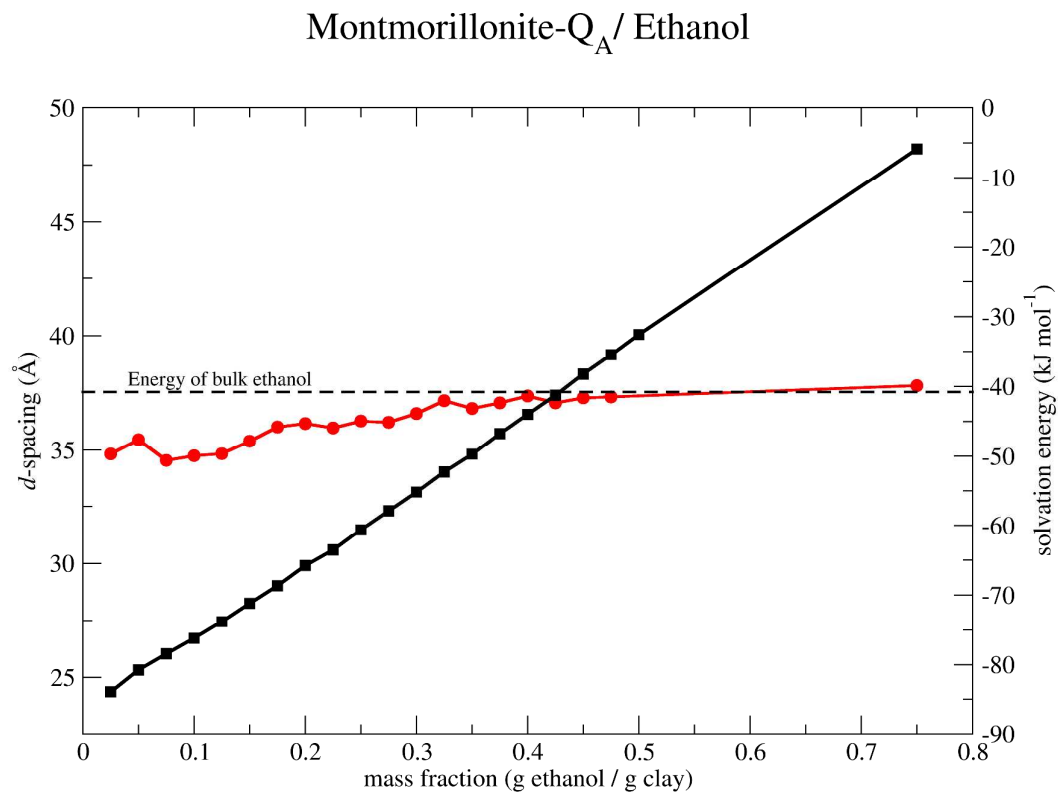


Figure S3: 1D-plot for MMT- Q_A with a solvent loading of 750 mg ethanol per g MMT- Q_A

MMT-Q_A / Ethanol, 750 mg/g clay

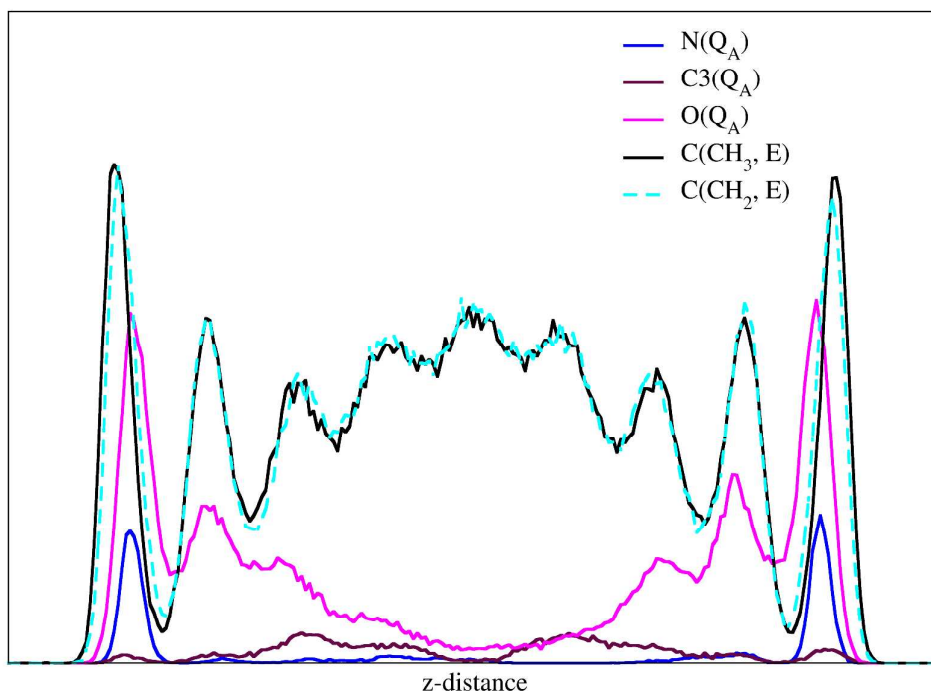


Figure S4: 1D-plot for MMT-Q_A with a solvent loading of 750 mg ethanol per g MMT-Q_A.

1. *International Organisation of Legal Metrology*; International Alcoholometric Tables. **1973**.
2. Jorgensen, W. L.; Maxwell, D. S.; Tirado-Rives, J.; Development and Testing of the Opls All-Atom Force Field on Conformational Energetics and Properties of Organic Liquids. *J. Am. Chem. Soc.* **1996**, *118*, 11225-11236.
3. Suter, J.; Coveney, P.; Anderson, R.; Greenwell, H.; Cliffe, S.; Rule Based Design of Clay-Swelling Inhibitors. *Energy Environ. Sci.* **2011**, *4*, 4572-4586.
4. Wang, J.; Kalinichev, A. G.; Kirkpatrick, R. J.; Hou, X.; Molecular Modeling of the Structure and Energetics of Hydrotalcite Hydration. *Chem. Mater.* **2001**, *13*, 145-150.